Spectrochimica Acta Part A: Molecular and Biomolecular Spectroscopy 274 (2022) 121107

Contents lists available at ScienceDirect

Spectrochimica Acta Part A: Molecular and Biomolecular Spectroscopy

journal homepage: www.elsevier.com/locate/saa

Temperature effect on vibrational properties of crystalline Dibenz[a,h] anthracene

Xiao-Miao Zhao [a,b,*], Yong-Kai Wei [c], Kai Zhang [d,e], Zhi-Wei Zhao [a,b,*], Shun Wang [a], Wei Miao [a], Su-Xuan Du [a], Shi-Jie Zhang [a], Wen-Feng Li [a], Chun-Long Guan [a], Li-Ping Shi [f], Xin-Po Lu [a], San-Kui Xu [a]

[a] College of Materials Science and Engineering, Henan University of Technology, Zhengzhou 450001, China
[b] Henan Province Engineering Research Center of New Cermet Matrix Composites, Zhengzhou 450001, China
[c] College of Science, Henan University of Technology, Zhengzhou 450001, China
[d] Key Laboratory of Materials Physics, Institute of Solid State Physics, Chinese Academy of Sciences, Hefei 230031, China
[e] Center for High Pressure Science and Technology Advanced Research, Shanghai 201203, China
[f] National Key Laboratory of Science and Technology on Advanced Composites in Special Environments, Harbin Institute of Technology, Harbin 150001, China

HIGHLIGHTS

- The temperature dependent Raman spectra of Dibenz[a,h]anthracene have been measured.
- A disorder-order phase transition occurred in Dibenz[a,h]anthracene upon cooling.
- The lattice modes exhibit significant anomalies at the transition temperature.
- The transition may result from the change of the tilt angle between the molecules.

GRAPHICAL ABSTRACT

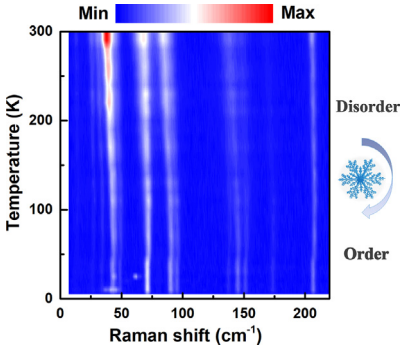

ARTICLE INFO

Article history:
Received 30 November 2021
Received in revised form 28 February 2022
Accepted 1 March 2022
Available online 3 March 2022

Keywords:
Dibenz[a,h]anthracene
Raman spectroscopy
Vibrational properties
Low temperature

ABSTRACT

Vibrational properties associated with the intra- and intermolecular bonding of the crystalline Dibenz[a,h]anthracene at low temperatures are investigated by Raman scattering. A complete characterization of phonon spectra is given for this material. In the 120–150 K temperature region, several lattice modes show abrupt changes of splitting and the discontinuities in the temperature shift, but no emergence of new modes. Moreover, the intensity ratio of $I_{68}/_{38}$ is greater than 1 below 130 K. Meanwhile, the aromatic C-C stretching modes exhibit anomalous behaviors in frequencies, widths, and intensities at about 130 K. These spectroscopic results demonstrate a disorder-order transition occurred at about 130 K. However, the modes, corresponding to C-H out-of-plane bending, C-H in-plane bending, and/or C-H rocking, have no significant change in the whole temperature range. It indicates that the transition mainly results from the change of the tilt angle between the molecules. Our work is of great significance to understand the internal vibrational properties of Dibenz[a,h]anthracene, and it also provides considerable supports for the further study of this material.

1. Introduction

Polycyclic aromatic hydrocarbons (PAHs) such as naphthalene, anthracene, and Dibenz[a,h]anthracene, consisting of extended π-

* Corresponding authors at: College of Materials Science and Engineering, Henan University of Technology, Zhengzhou 450001, China.
E-mail addresses: zhaoxiaomiao88@163.com (X.-M. Zhao), zhiwei_zhao@haut.edu.cn (Z.-W. Zhao).

https://doi.org/10.1016/j.saa.2022.121107
1386-1425/

conjugation, have various potential applications in optoelectronic, organic sensors, organic light emitting diods due to their high chemical stability, high charge-carrier mobility, and good fluorescence properties [1–7]. In previous studies, Ginzburg suggested the possible realization of high superconducting transition temperature (T_c) and even room temperature superconductivity in organic materials with a crystal structure made primarily of a complex network based on carbon and/or hydrogen [8]. The PAHs' electronic structure with π electron networks can be modified by metal doping, superconductivity having been found in the potassium-doped picene ($C_{22}H_{14}$) materials [9]. Motivated by this discovery, several PAHs become superconducting after the intercalation of alkali metal atoms, for example phenanthrene ($C_{14}H_{10}$), coronene ($C_{24}H_{12}$), and 1,2:8,9-dibenzopentacene ($C_{30}H_{18}$) [10–13]. The T_c was found to increase dramatically from 5 K to 33 K with increasing molecular chain length. Theoretical research showed that molecular edge structures as well as molecular sizes are closely related to the strength of electron–phonon coupling and T_cs [14]. Besides, high-temperature superconductivity in hydrogen-rich materials has been reported in several systems at high pressures [15–17]. Recently, near-room temperature superconducting transition (at approximately 288 K) has been reported lately in carbonaceous sulfur hydride at about 270 GPa [18]. A number of theoretical works have been carried out to investigate the underlined superconducting mechanism in hydrogen-containing materials due to the electron–phonon interactions [19–23]. Knowledge of the physical and vibrational properties of these material is helpful to understand the electron–phonon coupling.

Raman spectroscopy is a well-known tool for the observation of vibrational excitations in materials, especially organic materials [24–26]. Experimental studies have found that the edge structure, armchair or zigzag, of the organic molecule may play an important role in superconductivity of PAHs, the armchair edge is thought to be a key factor for superconductivity [12]. Thus, we have chosen one of PAHs, Dibenz[a,h]anthracene ($C_{22}H_{14}$) with armchair edge, to explore the vibrational properties. Dibenz[a,h]anthracene is the isomorphic alloisomer material of picene and is being examined as a potential candidate for exploring its superconductivity. Pure Dibenz[a,h]anthracene possesses othorhombic symmetry with four molecules per unit cell, the space group *Pcab* and lattice parameters: a = 8.263(2) Å, b = 11.466(2) Å, c = 15.238(2) Å [27]. Dibenz[a,h]anthracene is a wide band gap insulator with a band gap about 3.3 eV and its physical properties are similar to picene [19]. Furthermore, Dibenz[a,h]anthracene nanoaggregates possesses the exceptionally long singlet exciton diffusion length and superradiant property, which makes it a promising material for potential applications [28]. Besides, Dibenz[a,h]anthracene exhibits unusual physical, chemical, unreactive/reactive, bioaccumulating and carcinogen properties, and has been exploited in the process of bioremediation due to its unique physicochemical properties [29–30]. In general, the Dibenz[a,h]anthracene molecule was found to consist of parts having resemblance with anthracene as well as phenanthrene molecules. It has been well established that phenanthrene undergoes a disorder–order type of phase transition at around 200 K [31]. However, in contrast to the other two materials, little attention has been paid toward Dibenz[a,h]anthracene. The theoretical models suggest that the electron–electron correlations play an important role in doped PAHs. It is important for understanding the intermolecular interaction and electron–phonon interaction of Dibenz[a,h]anthracene,

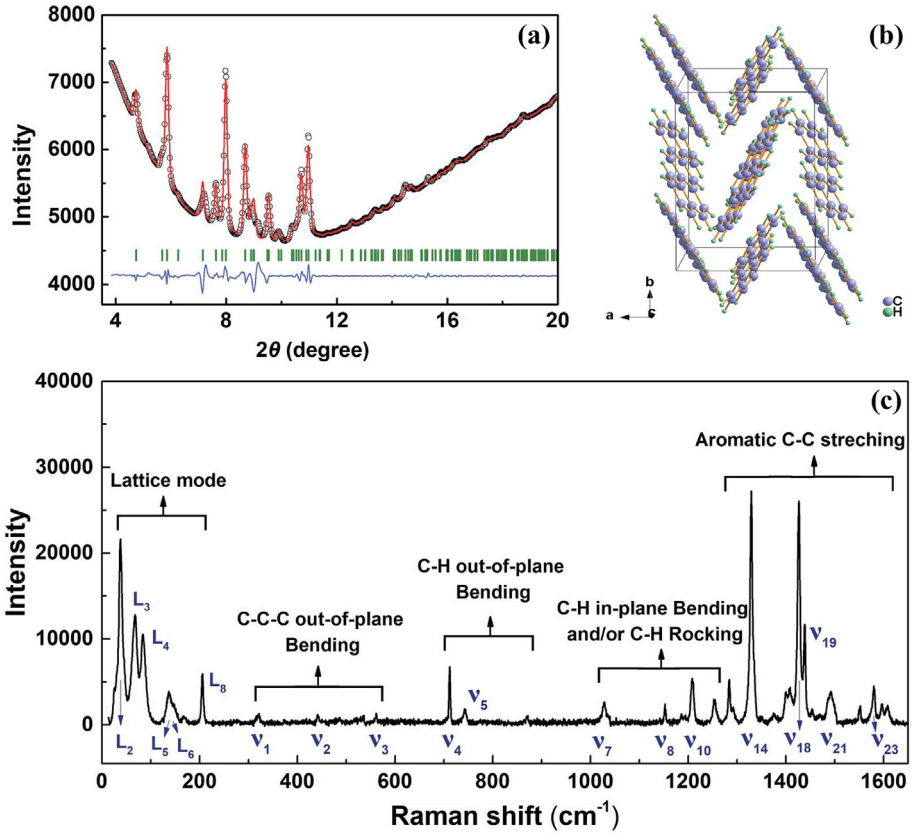

Fig. 1. (a) X-ray powder diffraction patterns of Dibenz[a,h]anthracene at room temperature. The open circles represent the measured intensities and the red lines the results of profile refinements by the best Le Bailfit with the space group of *Pcab*. The positions of the Bragg reflections are marked by vertical lines and the difference profiles are shown at the bottoms (blue lines). The *R* values are R_p = 0.68%, R_{wp} = 0.30% for the fitting. (b) Crystal structure of pristine solid Dibenz[a,h]anthracene, solid lines delineate unit cells [27]. (c) Raman spectra of Dibenz[a,h]anthracene at 300 K, measured with 660 nm laser excitation. Classifications of the vibration modes over the spectrum of 300 K are taken from Ref. [39–40]. (For interpretation of the references to colour in this figure legend, the reader is referred to the web version of this article.)

thus, a thorough study focused on the molecular vibrational properties of Dibenz[a,h]anthracene is highly desirable.

In this work, we measured the temperature dependent Raman spectra of Dibenz[a,h]anthracene from 5 to 300 K. The temperature effects on the vibrational modes from the lattice vibrations to the high-frequency modes are studied in detail. The results reveal a disorder–order phase transition occurred in Dibenz[a,h]anthracene at approximately 130 K. We compare the temperature dependence of the vibrational modes located in different frequency regions, and speculate that the transition may result from the change of the tilt angle between the molecules. Our work provides a basis for the further studies on Dibenz[a,h]anthracene.

2. Experimental details

High-purity Dibenz[a,h]anthracene was purchased from TCI Co. and used without further purification. The x-ray diffraction experiments at room temperature with synchrotron radiation were performed at the Shanghai Synchrotron Radiation Facility (SSRF). The wavelength of the x-ray is 0.6265 Å. The sample-to-detector distance and the image plate orientation angles were calibrated using CeO_2 standard. The two-dimensional diffraction images were converted to 2θ versus intensity data plots using the FIT2D software. The Rietveld fitting was performed using the GSAS package.

The sample was sealed in a quartz tube for Raman-scattering experiments in a glovebox maintained at moisture and oxygen levels below 0.1 ppm. An objective with X20 magnification (Mitutoyo) was used both for focusing the excitation light (660 nm) and for collecting the scattered light. The power was less than 1 mW before the objective to avoid possible damage of the sample. The 1800 lines/mm grating provides a spectral resolution of ~ 1 cm^{-1}. The Raman spectra were collected by a high-resolution (1024×1024) charge-coupled device designed by Princeton. The low-temperature conditions were obtained by using an in situ pressurized superfluid helium cryostat (CRYO). A continuous-flow liquid-helium cryostat was used to obtain a low-temperature condition from 5 to 300 K, and a vacuum pump was used to assist in achieving the temperature less than 40 K. Five accumulations with an exposure time of 20.0 *s* each were collected for all spectra. The spectra were collected from 10 to 1650 cm^{-1}.

3. Results and discussion

Raman scattering, which measures phonons (lattice and molecular vibrations) in Brillouin zone center, is known to be a powerful technique to detect phase transition or small structural distortion or the change of molecular configuration via the observation of the band splitting and/or soft modes [24–26]. First we performed x-ray diffraction measurements on Dibenz[a,h]anthracene. The results of measurement together with the structure refinement at room temperature are shown in Fig. 1(a). The diffraction data can be fit using the space group *Pcab* and the fitted results are in a good agreement with those in the literature [27]. The crystal structure and molecular structure of Dibenz[a,h]anthracene are shown in the inset of Fig. 1(b). In this study, we have measured the Raman spectrum of Dibenz[a,h]anthracene within the temperature from 5 to 300 K. The Raman spectra of Dibenz[a,h]anthracene at 300 K are presented in Fig. 1(c). The active modes were predicted from a group-theoretic analysis of Γ-point lattice vibrations of Dibenz [a,h]anthracene [32]. The irreducible representations for Dibenz [a,h]anthracene are $\Gamma = 36\ A_g + 18\ B_g + 18\ A_u + 36\ B_u$. The infrared spectrum possesses 29 B_u and 7 A_u [33]. Based on the analysis of molecular structure, it is clear that the vibrational properties of Dibenz[a,h]anthracene are similar to those of polycyclic aromatic hydrocarbon [34–38]. The modes assignments for Dibenz[a,h]anthracene are depicted over the spectrum at 300 K in Fig. 1 [39,40].

Raman spectra of Dibenz[a,h]anthracene collected at low temperatures down to 5 K are shown in Fig. 2. For organic molecules the lattice and intramolecular vibrational modes are situated in different wavenumber regions. For clarity, the Raman spectra could be divided into two regions shown in Fig. 2(a), (b). In the low wavenumber range, we observed a great variety of Raman bands arising from the lattice modes of the sample. When looking at the evolution of the Raman spectra as a function of temperature, the lattice modes exhibit distinct changes in the number, intensity, and sharpness of peaks. At high temperatures, the lattice modes in the Dibenz[a,h]anthracene show very broad features and often overlap to some indistinguishable peaks. With decreasing temperature down to 130 K, a shoulder peak appears on the high-wavenumber side of L_2, and the vibrational mode gradually separates from the L_2 mode with the decrease of temperature. Interestingly, the intensity of the L_2 mode is higher than L_3 at ambient temperature, however, the mode L_2 gains intensity rapidly as temperature is decreased and is stronger than the mode L_3 below

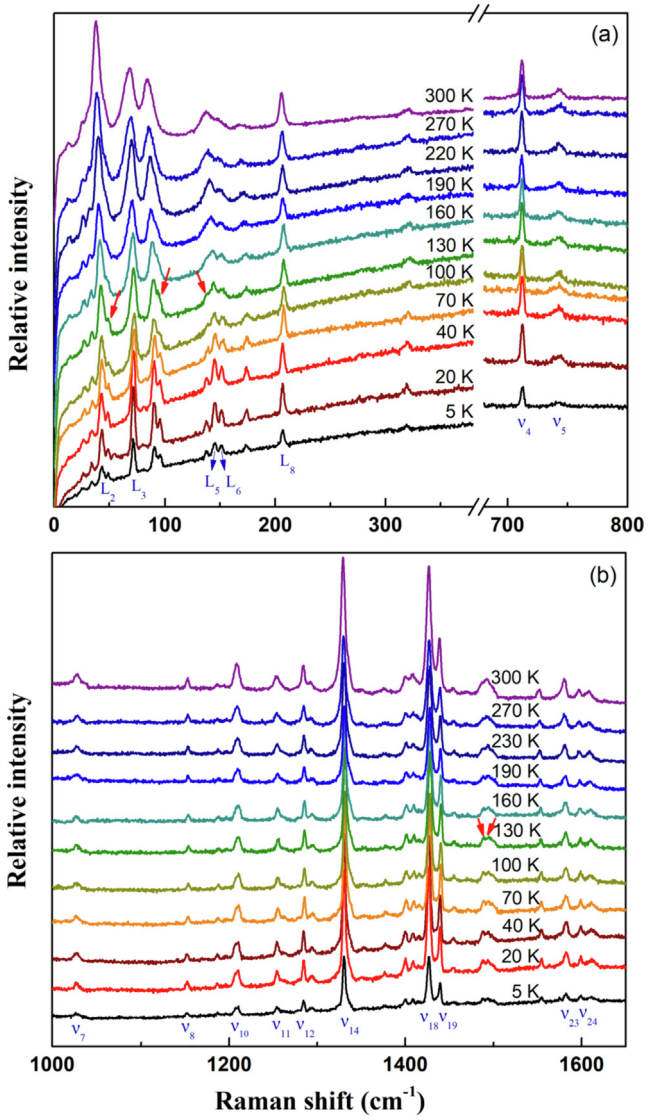

Fig. 2. (a) Representative Raman spectra of Dibenz[a,h]anthracene in the low wavenumber range of 10–800 cm^{-1}, (b) Selected Raman spectra of Dibenz[a,h] anthracene in the high wavenumber range of 1000–1650 cm^{-1}. The arrows indicate the changes of Raman modes.

130 K. This behavior points to the exchange of the symmetry of the two modes and may result from Fermi resonance [41]. In addition to this, the broad peak at 84 cm^{-1} splits into two separate modes at 130 K. Meanwhile, a shoulder peak on the low- wavenumber side of L_5 obviously raises in Raman spectra. At low temperatures, one can clearly see that the spectra show obvious splits on some peaks. However, we observed that the Raman spectra between 210 and 1250 cm^{-1} show a subtle change with decreasing temperature. In this spectral region, the C-C-C out of plane bending modes are located in the spectra region between 210 and 600 cm^{-1}. The region of 680–1000 cm^{-1} is characterized by the C-H out of plane bending, while the C-H in-plane bending and/or C-H rocking modes can be seen in the interval of 1000–1250 cm^{-1}. In the high wavenumber regions, the peak located at around 1500 cm^{-1} loses its degeneracy and splits into two modes below 130 K. The behavior of Raman spectra of Dibenz[a,h]anthracene as a function of temperature is very similar to that of p-oligophenyls [42]. As the temperature decreases, there is an obvious splitting for the broad peaks, especially the lattice modes. Moreover, most of the full widths at half maximum (FWHMs) of the vibrational modes decrease as temperature is decreased [25]. These features in the Raman spectra suggest the substantial changes may occur in this region of 120–150 K. In the whole temperature range, no new peak emerges. This indicates that this transition belongs to order–disorder transition or molecular-conformation change.

Details of the temperature evolution of the Dibenz[a,h]anthracene Raman spectra in the lattice vibration range are shown in Fig. 3. In order to analyze the Raman spectrum accurately, a constant background was removed from the raw data. The scattering intensities have been normalized by $I\ (w) = I_0\ (w) / [\ n\ (w, T) + 1]$. Where $n\ (w, T)$ is the Bose–Einstein distribution function evaluated at mode energy w and temperature T, and $I_0\ (w)$ is the observed intensity. Fig. 3(a) shows the temperature-dependent Raman intensity map of Dibenz[a,h]anthracene (upper panel) and the Raman spectra at 5 K and 300 K (lower panel). We can observe that the wavenumbers of all the observed Raman bands have progressive upshifts, and the linewidths become narrowed with decreasing temperature from 300 to 130 K. Meanwhile, some lattice modes show a clear splitting at around 130 K. The wavenumbers of lattice modes are almost stable below 120 K. Comparing with the Raman spectra at 300 K, the number of Raman spectra at 5 K has an obvious change, which is result from the splitting of the intermolecular modes. The splitting of lattice modes is a good indicator of the disorder–order transition. Based on the above analysis, we can infer that the transition may belong to order–disorder transition without structural modulation.

In order to precisely determine the temperature at which the order–disorder transitions take place, the temperature dependencies of lattice modes have been plotted out in Fig. 3(b). The lattice modes L_2 and L_5 show a dramatic increase in frequency with decreasing the temperature at first. At around 150 K, the bands L_2 and L_5 split into two modes, respectively, and then have a smaller change below 120 K. The lattice modes L_6 and L_8 show an interesting behavior where the wavenumber position first increases sharply with decreasing temperature, and then decreases with decreasing temperature after evolving through a maximum value at around 130 K. It is clear that there is an obvious discontinuity in the data at around 130 K confirming our conclusion of temperature induced transitions.

Now paying attention to the singe peak L_3, one can clearly see from Fig. 3(c) that the FWHM of lattice mode L_3 is about 12 cm^{-1} at room temperature. With decreasing temperature, the FWHM of lattice mode L_3 exhibits a monotonous decrease (0.035 cm^{-1}/K). However, the lattice mode L_3 decreases with the rate 0.024 cm^{-1}/K below 130 K. A discontinuity of the FWHM of lattice mode L_3 occurs in the temperature region 120–150 K. It can be interpreted that the temperature-induced FWHM narrowing may reflect the decreased anharmonic effect of the phonons after entering into the ordered state [43–45]. The intensity of the mode L_2 is much stronger than the mode L_3 at 300 K from the lower panel of

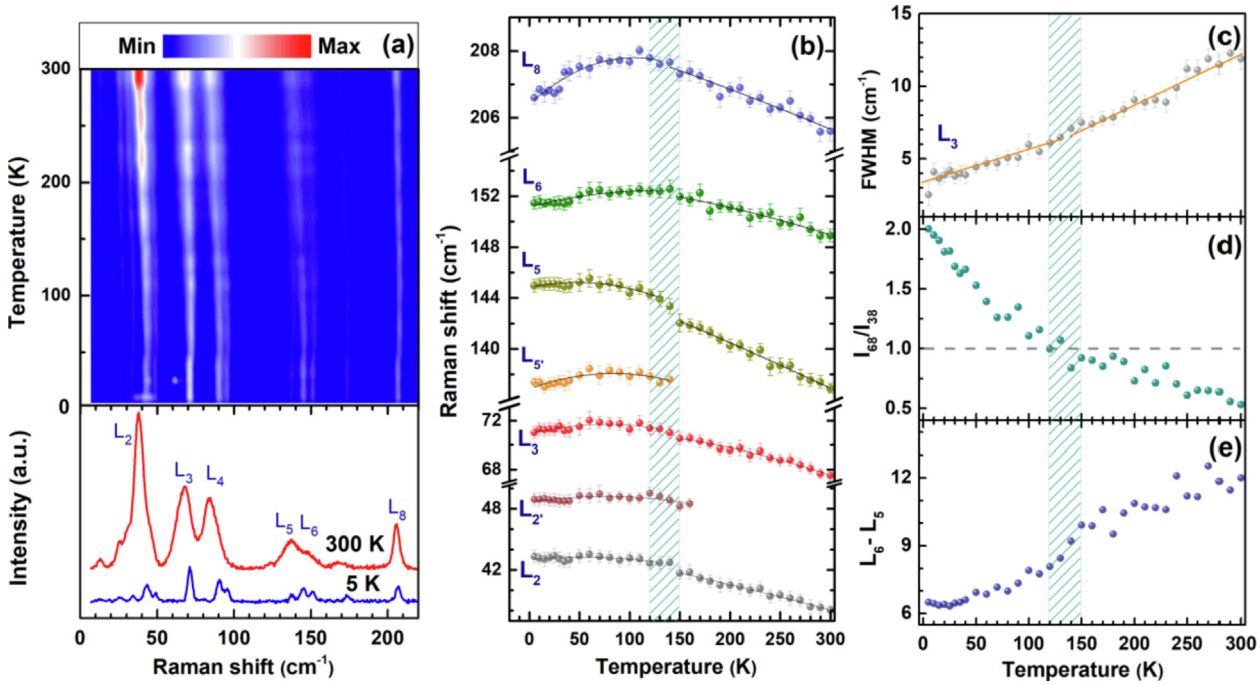

Fig. 3. (a) Raman spectra map of the low energy modes of Dibenz[a,h]anthracene. The spectra at 5 K and 300 K are shown for clarity. (b) Temperature dependence of the peak positions observed in Dibenz[a,h]anthracene in the low wavenumber range of 10–210 cm^{-1}. These solid lines are drawn to guide the eyes. (c) FWHM of the L_3 mode as functions of temperature. (d) Temperature dependence of Raman intensity ratio I68/I38 of the Raman peaks at 68 cm^{-1} and at 38 cm^{-1}. (e) The difference of the L_6 and L_5 as a function of temperature. The shadow areas indicate the phase boundaries.

Fig. 3(a), however, at 5 K it exhibits a reverse tendency. Fig. 3(d) shows the Raman intensity ratios for the selected modes as a function of temperature. The intensity ratio of $I_{68}/_{38}$ is less than 1 below 130 K, possibly due to the exchange of the symmetry of the modes or the unsaturated carbon converting into saturated carbon. The inflexion of the tendency is found around 130 K, which is consistent with the order–disorder transition point. Additionally, the wavenumber difference between the L_6 and the L_5 peak positions is presented in Fig. 3(e), which is about 12 cm^{-1} at 300 K. It decreases consecutively with decreasing temperature and almost saturates at 7 cm^{-1} below 120 K, also providing evidence of the order–disorder transition at around 130 K. The temperature evolution behavior of Dibenz[a,h]anthracene in lattice modes is similar to that of p-quaterphenyl [46]. Below the transition temperature, most of the lattice peaks exhibit a clear splitting. The low energy peaks first rapidly increase in wavenumber position with decreasing temperature, and then have a subtle change below the transition temperature. Moreover, their FWHM exhibit a sudden drop above the transition temperature. Zhang et al. [46] indicated that the dramatic changes in the widths, intensity, and the splits of the lattice modes mainly result from the order–disorder transition taking place in p-quaterphenyl. A similar feature is observed in the Raman spectrum of Dibenz[a,h]anthracene. Thus, it can be inferred that the order–disorder phase transition occurs between 120 and 150 K in Dibenz[a,h]anthracene.

Fig. 4(a) shows the Raman spectra of Dibenz[a,h]anthracene at various temperatures down to 5 K in the range between 680 and 780 cm^{-1}. Over the whole temperature range, the modes have no significant change in intensity and peak position. The detailed temperature dependencies of ν_4 and ν_5 modes have been plotted out in Fig. 4(b). The mode at frequency of 712 cm^{-1}, corresponding to C-H out-of-plane bending, keeps almost constant value upon cooling. Another C-H out-of-plane bending mode located at 744 cm^{-1} fluctuates between 744 and 742 cm^{-1}, but almost stabilizes at low temperatures. The evolution behavior at low temperatures of the four modes of ν_8, ν_9, ν_{10} and ν_{11}, associated with C-H in-plane bending and/or C-H rocking, are depicted in Fig. 4(c) and (d). The figures show that the four modes of ν_8, ν_9, ν_{10} and ν_{11} are found be to stable at low temperatures except some subtle changes in wavenumber position. Based on the change of vibrational modes, we can infer that the effects of temperature on the molecular arrangement is larger than on the molecular shape.

We now focus our attention on higher wavenumber region (see Fig. 5). The region of 1250–1650 cm^{-1} is characterized by the aromatic C-C stretching. The fitted peak position and FWHM of the mode ν_{14} are shown in Fig. 5(a). The peak position of mode ν_{14} exhibits a pronounced rise as temperature decreases, reaches a maximum of 1331.8 cm^{-1} at 140 K, and then shows a negative wavenumber shift upon cooling. It is worth noting that the FWHM of vibrational mode ν_{14} has a drastic decrease with decreasing

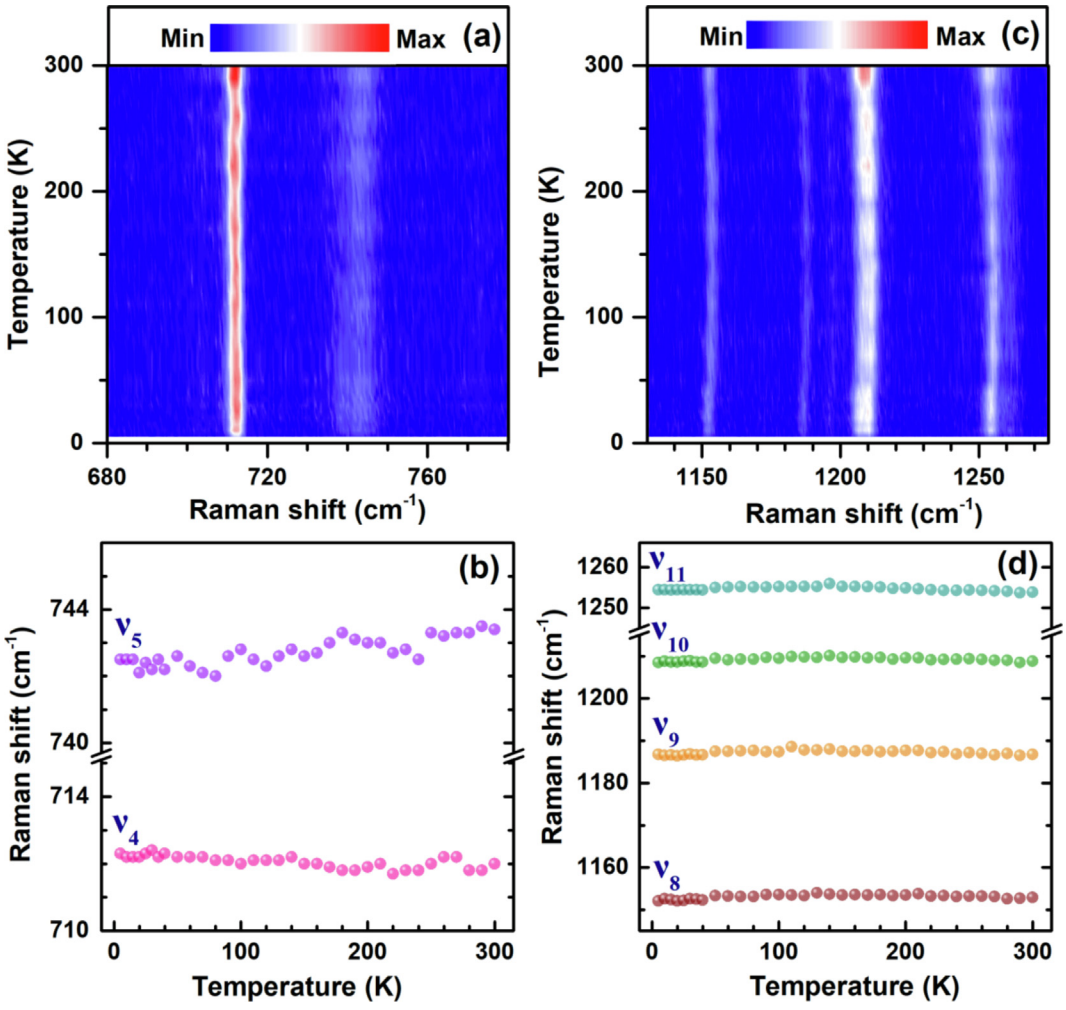

Fig. 4. (a) Raman spectra map of Dibenz[a,h]anthracene in the wavenumber range 680–780 cm^{-1}. (b) Peak positions of the ν_4 mode and the ν_5 mode as functions of temperature. (c) Raman spectra map of Dibenz[a,h]anthracene in the wavenumber range around 1200 cm^{-1}. (d) Temperature dependent Raman peak positions of several vibrons of crystalline Dibenz[a,h]anthracene.

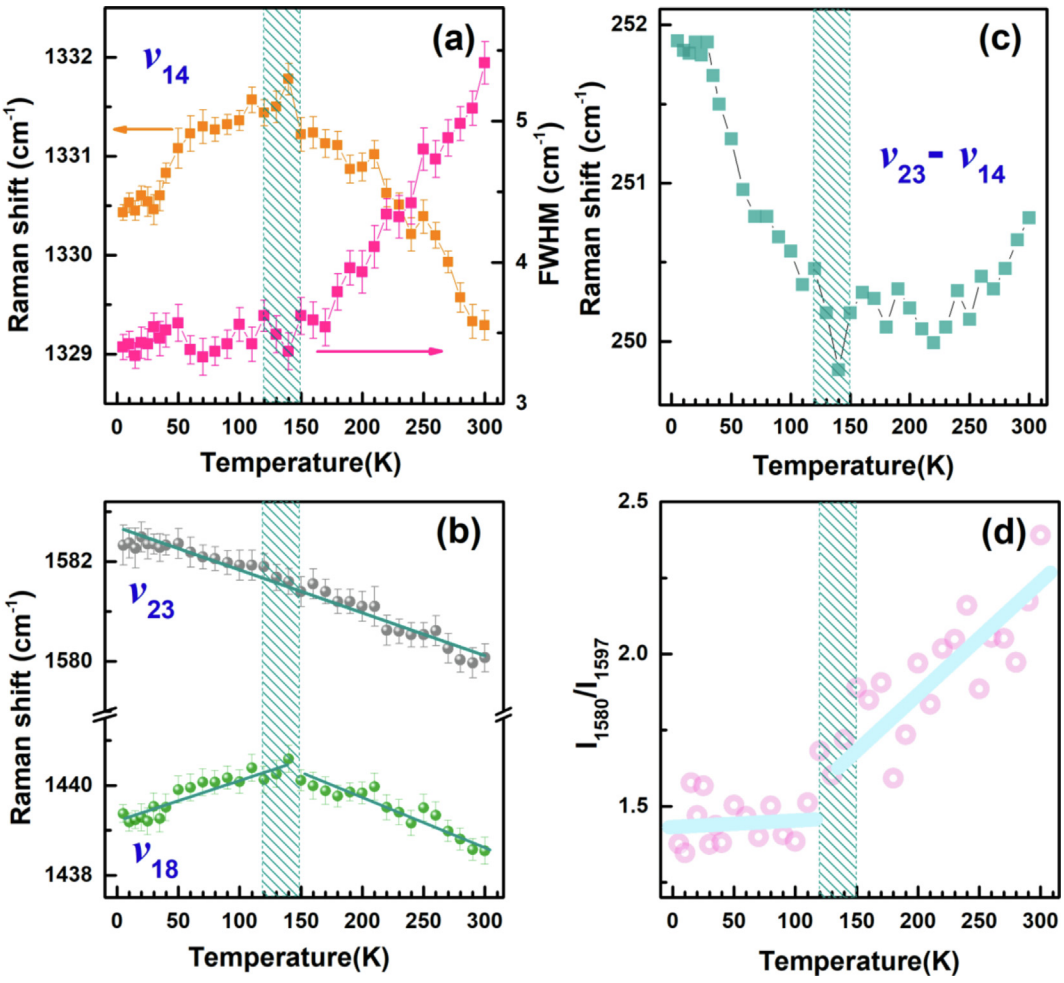

Fig. 5. (a) Peak positions and FWHM of the vibrational modes ν_{14} as a function of temperature. (b) Temperature dependent peak positions of the two peaks at around 1480 and 1580 cm^{-1}. (c) Temperature dependent peak positions difference between ν_{23} and ν_{14}. (d) Intensity ratios of the lower energy peak at 1580 cm^{-1} and the higher energy peak at 1597 cm^{-1} as a function of temperature.

temperature, then becomes almost constant below 130 K. This provides further evidence for an order–disorder transition taking place around 130 K. Meanwhile, one can see from Fig. 5(b) that the internal mode of ν_{18} shows a similar trend as that of ν_{14} at low temperatures. However, the mode of ν_{23} shows a smooth and stable blue-shift with decreasing temperature. The calculated position difference ν_{23}-ν_{14} of Dibenz[a,h]anthracene is shown in Fig. 5(c). The difference gradually starts to decrease with decreasing temperature, and then shows a sudden increase when the temperature drops to 140 K. This scenario is well in accord with the order–disorder transition case. The intensity of the peak located at 1597 cm^{-1} increases with decreasing temperature, whereas the peak at 1580 cm^{-1} almost stabilizes its intensity. The intensity ratio of $I_{1597}/_{1580}$ is about 2.5 at 300 K, as shown in Fig. 5(e). One can clearly see that the intensity ratio of $I_{1597}/_{1580}$ rapidly decreases with decreasing temperature. After entering into the ordered state, we detected a modest decrease of the intensity ratio of $I_{1597}/_{1580}$ upon further cooling. The dramatic changes of the aromatic C-C stretching modes also illustrate any possible phase transitions occurring within the sample in the region 120–150 K [24]. It is important to point out that the changes of the aromatic C-C stretching modes are more obvious than that of C-H out-of-plane bending, C-H in-plane bending, and/or C-H rocking modes at low temperatures. This phenomenon indicates that a decrease in temperature has a significant impact on the tilt angle between the molecules. The reemergence of the tilt angle between the molecules also occurs in similar aromatic hydrocarbons triphenylene under pressure [37]. The combined experimental and computational study on triphenylene reveals that the angles between the molecules as a function of pressure have a kink at 6.0 GPa, coinciding with the change of lattice modes at about 6.0 GPa. The anomaly of angles between the molecules at high pressures yields to the change of lattice modes.

In addition to this, N. J. Tro et al. [31] reported that phenanthrene (three rings) undergoes a disorder-to-order transition at 200 K from the sudden changes in the absorption and fluorescence spectra, while the disorder-to-order transition take place at about 130 K in Dibenz[a,h]anthracene (five rings). Benzene is suggested to have no disorder-to-order transition below 300 K. Based on these findings, it can be determined that the transition temperature decreases with increasing number of benzene rings, which may result from the gradual decrease of the tilt angle between the molecules with increasing molecular chain length. Previous studies found that superconductivity in aromatic hydrocarbons can be achieved by alkali metal doping. Furthermore, the superconducting transition temperature of hydrocarbon superconductors is found to substantially increase with increasing number of benzene rings. There is a connection between the reemergence of the tilt angle between the molecules and the properties at low temperatures. A study of the spectrum at low temperatures is helpful to understand the properties and mechanism of superconductivity in aromatic hydrocarbons.

4. Conclusion

In conclusion, we have investigated the vibrational properties of Dibenz[a,h]anthracene by Raman scattering measurements from 5 K to 300 K. Comprehensive analysis of the intra- and intermolecular vibrational modes has been completed to understand the phonon behaviors. The modes located in the librational motion range all shift toward higher frequency with decreasing the temperature. Below 130 K, the spectra show the splitting of bands, the discontinuities in the temperature shift, and the changes in FWHM of modes. Meanwhile, the modes, corresponding to aromatic C-C stretching, show a slope change in frequency and intensity ratio. These experimental results reveal a disorder–order transition occurred between 120 and 150 K without structural modulation. For the intramolecular modes, the anomalies mainly focus on the modes with higher frequencies. Over the whole temperature range, the modes, associated with C-H out-of-plane bending and C-H in-plane bending and/or C-H rocking, have no significant change. We can reasonably speculate that a decrease in temperature has a significant impact on the tilt angle between the molecules. These findings at low temperatures are of great importance for understanding the physical properties in Dibenz[a,h]anthracene.

CRediT authorship contribution statement

Xiao-Miao Zhao: Data curation, Formal analysis, Investigation, Writing – original draft, Writing – review & editing. **Yong-Kai Wei:** Data curation, Formal analysis. **Kai Zhang:** Data curation, Formal analysis. **Zhi-Wei Zhao:** Supervision, Writing – review & editing. **Shun Wang:** Writing – review & editing. **Wei Miao:** Writing – review & editing. **Su-Xuan Du:** Writing – review & editing. **Shi-Jie Zhang:** Writing – review & editing. **Wen-Feng Li:** Writing – review & editing. **Chun-Long Guan:** Writing – review & editing. **Li-Ping Shi:** Writing – review & editing. **Xin-Po Lu:** Writing – review & editing. **San-Kui Xu:** Writing – review & editing.

Declaration of Competing Interest

The authors declare that they have no known competing financial interests or personal relationships that could have appeared to influence the work reported in this paper.

Acknowledgment

The research was supported by the Key Scientific and Technological Research Projects in Henan Province (Grant No. 212102210114 and 202102210217) and the Doctoral Fund of Henan University of Technology (Grant No. 2018BS004) and the Fundamental Research Funds for the Henan Provincial Colleges and University of Technology (Grant No. 2018QNJH29) and the Cultivation Programme for Young Backbone Teachers in Henan University of Technology, and the science foundation of national key laboratory of science and technology on advanced composites in special environments (Grant No.6142905203114).

References

[1] A. Naibi Lakshminarayana, A. Ong, C. Chi, Modification of acenes for n-channel OFET materials, J. Mater. Chem. C 6 (14) (2018) 3551–3563.
[2] X. Feng, J.-Y. Hu, C. Redshaw, T. Yamato, Functionalization of pyrene to prepare luminescent materials–Typical examples of synthetic methodology, Chem. Eur. J. 22 (34) (2016) 11898–11916.
[3] X. Li, L. Yang, L. Zhao, X.L. Wang, K.Z. Shao, Z.M. Su, Luminescent metal–organic frameworks with anthracene chromophores: small-molecule sensing and highly selective sensing for nitro explosives, Cryst. Growth Des. 16 (2016) 4374–4382.
[4] J. Huang, J.-H. Su, H.e. Tian, The development of anthracene derivatives for organic light-emitting diodes, J. Mater. Chem. 22 (22) (2012) 10977, https://doi.org/10.1039/c2jm16855c.
[5] J. Sinova, A. S. N'unez, J. Schliemann, A. H. MacDonald, Electron–phonon interactions in polyacene organic transistors, Phys. Status Solidi B 230 (2002) 309–313.
[6] T. Minakata, Fabrication of a gas sensor using pentacene thin films as a detector, polym, Adv. Technol. 6 (9) (1995) 607–610.
[7] T.W. Kelley, P.F. Baude, C. Gerlach, D.E. Ender, D. Muyres, M.A. Haase, M.A. Vogel, S.D. Theiss, Recent progress in organic electronics: materials, devices, and processes, Chem. Mater. 16 (2004) 4413–4422.
[8] V.L. Ginzburg, High-temperature superconductivity-dream or reality?, Phys Usp. 19 (1976) 174–179.
[9] R. Mitsuhashi, Y. Suzuki, Y. Yamanari, H. Mitamura, T. Kambe, N. Ikeda, H. Okamoto, A. Fujiwara, M. Yamaji, N. Kawasaki, Y. Maniwa, Y. Kubozono, Superconductivity in alkali-metal-doped picene, Nature (London) 464 (7285) (2010) 76–79.
[10] X.F. Wang, R.H. Liu, Z. Gui, Y.L. Xie, Y.J. Yan, J.J. Ying, X.G. Luo, X.H. Chen, Superconductivity at 5 k in alkali-metal-doped phenanthrene, Nat. Commun. 2 (2011) 507.
[11] Y. Kubozono, H. Mitamura, X. Lee, X. He, Y. Yamanari, Y. Takahashi, Y. Suzuki, Y. Kaji, R. Eguchi, K. Akaike, T. Kambe, H. Okamoto, A. Fujiwara, T. Kato, T. Kosugi, Hi. Aoki, Metal-intercalated aromatic hydrocarbons: a new class of carbon-based superconductors. Phys. Chem. Chem. Phys. 13 (2011) 16476–16493.
[12] M. Xue, T. Cao, D. Wang, Y. Wu, H. Yang, X. Dong, J. He, F. Li, G.F. Chen, Superconductivity above 30 k in alkali-metal-doped hydrocarbon, Sci. Rep. 2 (2012) 389–392.
[13] Q.W. Huang, G.H. Zhong, J. Zhang, X.M. Zhao, C. Zhang, H.Q. Lin, X. j., Chen Constraint on the potassium content for the superconductivity of potassium-intercalated phenanthrene, J. Chem. Phys. 140 (2014) 114301.
[14] T. Kato, K. Yoshizawa, K. Hirao, Electron–phonon coupling in negatively charged acene-and phenanthrene-edge-type hydrocarbon crystals, J. Chem. Phys. 116 (2002) 3420–3429.
[15] A.P. Drozdov, M.I. Eremets, I.A. Troyan, V. Ksenofontov, S.I. Shylin, Conventional superconductivity at 203 kelvin at high pressures in the sulfur hydride system, Nature (London) 525 (7567) (2015) 73–76.
[16] M. Somayazulu, M. Ahart, A.K. Mishra, Z.M. Geballe, M. Baldini, Y. Meng, V.V. Struzhkin, R.J. Hemley, Evidence for superconductivity above 260 K in lanthanum superhydride at megabar pressures, Phys. Rev. Lett. 122 (2019) 027001.
[17] A.P. Drozdov, P.P. Kong, V.S. Minkov, S.P. Besedin, M.A. Kuzovnikov, S. Mozaffari, L. Balicas, F.F. Balakirev, D.E. Graf, V.B. Prakapenka, E. Greenberg, D.A. Knyazev, M. Tkacz, M.I. Eremets, Superconductivity at 250 K in lanthanum hydride under high pressures, Nature (London) 569 (7757) (2019) 528–531.
[18] E. Snider, N. Dasenbrock-Gammon, R. McBride, M. Debessai, H. Vindana, K. Vencatasamy, K.V. Lawler, A. Salamat, R.P. Dias, Room-temperature superconductivity in a carbonaceous sulfur hydride, Nature (London) 586 (7829) (2020) 373–377.
[19] G.H. Zhong, X.J. Chen, H.Q. Lin, Superconductivity and its enhancement in polycyclic aromatic hydrocarbons, Front. Phys. 7 (2019) 52.
[20] A. Subedi, L. Boeri, Vibrational spectrum and electron-phonon coupling of doped solid picene from first principles, Phys. Rev. B 84 (2011) 020508.
[21] T. Kato, T. Kambe, Y. Kubozono, Strong intramolecular electron-phonon coupling in the negatively charged aromatic superconductor picene, Phys. Rev. Lett. 107 (2011) 077001.
[22] C. Zhang, X.-J. Chen, H.-Q. Lin, Phase transitions and electron–phonon coupling in platinum hydride, J. Phys.: Condens. Matter 24 (3) (2012) 035701, https://doi.org/10.1088/0953-8984/24/3/035701.
[23] E.F. Talantsev, The electron-phonon coupling constant, Fermi temperature and unconventional superconductivity in the carbonaceous sulfur hydride 190 K superconductor, Supercond. Sci. Technol. 34 (2021) 034001.
[24] D.B. Menezes, A. Reyer, A. Marletta, M. Musso, Glass transition of polystyrene (PS) studied by Raman spectroscopic investigation of its phenyl functional groups, Mater. Res. Express 4 (2017) 015303.
[25] M. Musso, F. Matthai, D. Keutel, K. Oehme, Isotropic Raman line shapes near gas–liquid critical points: The shift, width, and asymmetry of coupled and uncoupled states of fluid nitrogen, J. Chem. Phys. 116 (2002) 8015–8027.
[26] D. Bertoldo Menezes, A. Reyer, A. Benisek, E. Dachs, C. Pruner, M. Musso, Raman spectroscopic insights into the glass transition of poly (methyl methacrylate), Phys. Chem. Chem. Phys. 23 (2) (2021) 1649–1665.
[27] J. Iball, C.H. Morgan, D.E. Zacharias, Refinement of the crystal structure of orthorhombic dibenz [a, h]-anthracene, J. Chem. Soc., Perkin Trans. 2 (1975) 1271–1272.
[28] B. Manna, A. Nandi, Exploration of photophysics and presence of Long singlet exciton diffusion length in dibenz [a, h] anthracene nanoaggregates, J. Photoch. Photobio. A 392 (2020) 112407.
[29] V. Vasudevan, K.V. Gayathri, M.E.G. Krishnan, Bioremediation of a pentacyclic PAH, Dibenz (a, h) Anthracene-A long road to trip with bacteria, fungi, autotrophic eukaryotes and surprises, Chemosphere 202 (2018) 387–399.
[30] C. Zhang, Y. Luo, R. Zhong, P.T.Y. Law, S.S. Boon, Z. Chen, C. Wong, P.K.S. Chan, Role of polycyclic aromatic hydrocarbons as a co-factor in human papillomavirus-mediated carcinogenesis, BMC cancer 19 (2019) 1–10.
[31] N.J. Tro, A.M. Nishimura, S.M. George, Disorder-order transition and energy transfer in phenanthrene adlayers on alumina, J. Phys. Chem. 93 (1989) 3276–3282.

[32] Y.L. Zeng, L. Jiang, X.Y. Cai, Y. Li, Identification of the characteristic vibrations for 16 PAHs based on Raman spectrum, Spectrosc. Spect. Anal. 34 (2014) 2999–3004.
[33] A.L. Mattioda, C.W. Bauschlicher, A. Ricca, J. Bregman, D.M. Hudgins, L.J. Allamandola, Infrared spectroscopy of matrix-isolated neutral polycyclic aromatic nitrogen heterocycles: The acridine series, Spectrochim. Acta A Mol. Biomol. Spectrosc. 181 (2017) 286–308.
[34] F. Capitani, M. Höppner, B. Joseph, L. Malavasi, G.A. Artioli, L. Baldassarre, A. Perucchi, M. Piccinini, S. Lupi, P. Dore, L. Boeri, P. Postorino, Combined experimental and computational study of the pressure dependence of the vibrational spectrum of solid picene $C_{22}H_{14}$, Phys. Rev. B 88 (2013) 144303.
[35] X.M. Zhao, J. Zhang, A. Berlie, Z.X. Qin, Q.W. Huang, S. Jiang, J.B. Zhang, L.Y. Tang, J. Liu, C. Zhang, G.H. Zhong, H.Q. Lin, X.J. Chen, Phase transformations and vibrational properties of coronene under pressure, J. Chem. Phys. 139 (2013) 144308.
[36] Q.W. Huang, J. Zhang, A. Berlie, Z.X. Qin, X.M. Zhao, J.B. Zhang, L.Y. Tang, J. Liu, C. Zhang, G.H. Zhong, H.Q. Lin, X.J. Chen, Structural and vibrational properties of phenanthrene under pressure, J. Chem. Phys. 139 (2013) 104302.
[37] X.M. Zhao, G.H. Zhong, J. Zhang, Q.W. Huang, A.F. Goncharov, H.Q. Lin, X.J. Chen, Combined experimental and computational study of high-pressure behavior of triphenylene, Sci. Rep. 6 (2016) 1–10.
[38] X.M. Zhao, Q.W. Huang, J. Zhang, G.H. Zhong, H.Q. Lin, X.J. Chen, High-pressure study of isoviolanthrone by raman spectroscopy, J Chem. Phys. 140 (2014) 244314.
[39] L. Colangeli, V. Mennella, G.A. Baratta, E. Bussoletti, G. Strazzulla, Raman and infrared spectra of polycyclic aromatic hydrocarbon molecules of possible astrophysical interest, Astrophys. J. 396 (1992) 369–377.
[40] E. Smith, G. Dent, Modern raman spectroscopy: a practical approach, John Wiley & Sons, 2019.
[41] Y. Lin, W.L. Mao, V. Drozd, J.H. Chen, L.L. Daemen, J. Chem. Phys. 129 (2008) 234509.
[42] K. Zhang, R.S. Wang, X.J. Chen, Order–disorder transition in p-oligophenyls, Phys, Chem, Chem, Phys 21 (2019) 13590–13599.
[43] A. Girard, H. Cailleau, Y. Marqueton, C. Ecolivet, Raman scattering study of the order-disorder phase transition in para-terphenyl, Chem. Phys. Lett. 54 (3) (1978) 479–482.
[44] G. Heimel, D. Somitsch, P. Knoll, E. Zojer, Albrecht theory and anharmonic coupling in polyphenyl raman spectra, Synth. Met. 139 (3) (2003) 823–825.
[45] A. Girard, M. Sanquer, Y. Dělugeard, Low-frequency Raman study of para-terphenyl: influence of the isotopic substitution and interpretation of the spectra in both phases, Chem. Phys. 96 (3) (1985) 427–434.
[46] K. Zhang, X.J. Chen, Temperature effect on vibrational properties of crystalline p-quaterphenyl, Spectrochim. Acta A 213 (2019) 199–203.